Supplementary Information

Persulfate enhanced ciprofloxacin removal from water by laser-induced graphene-based electroconductive ultrafiltration membrane

Najmul Haque Barbhuiya[1], Utkarsh Misra[2], Bhavana Kanwar[1], Swatantra P. Singh [1,2,3]*

[1] Environmental Science and Engineering Department (ESED), Indian Institute of Technology Bombay, Mumbai 400076, India

[2] Centre for Research in Nanotechnology & Science (CRNTS), Indian Institute of Technology Bombay, Mumbai 400076, India

[3]Interdisciplinary Program in Climate Studies, Indian Institute of Technology Bombay, Mumbai 400076, India

*Corresponding author's e-mail: swatantra@iitb.ac.in

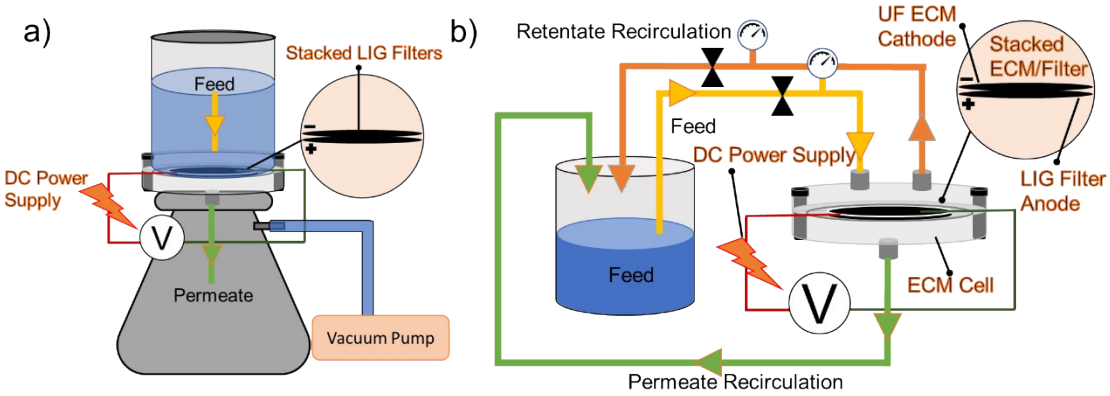

Fig S1: Schematics of the filtration system used in the study; a) dead-end filtration mode and b) crossflow filtration mode.

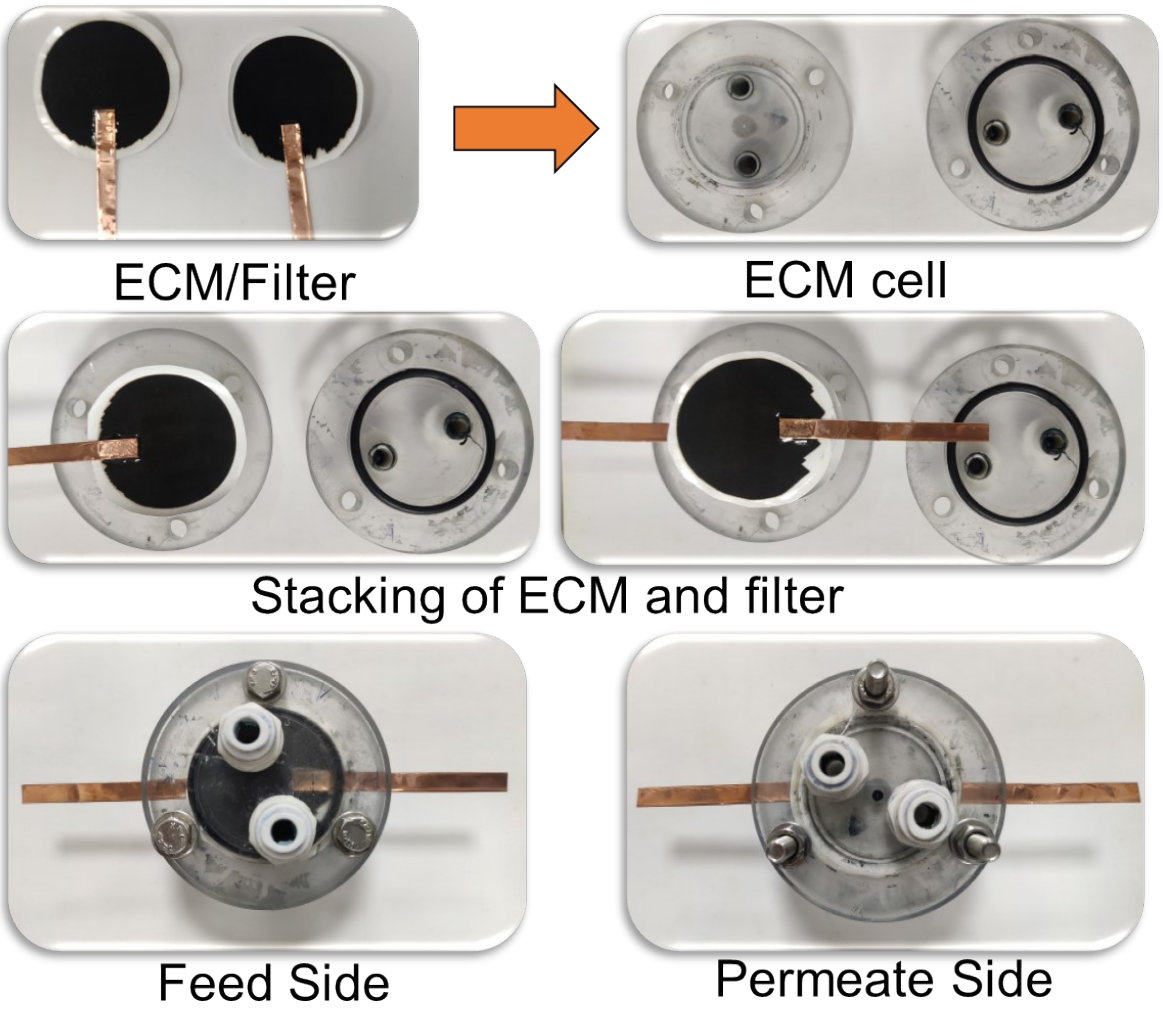

Fig S2: Photograph of ECM/filter stack and their placement in the ECM cell.

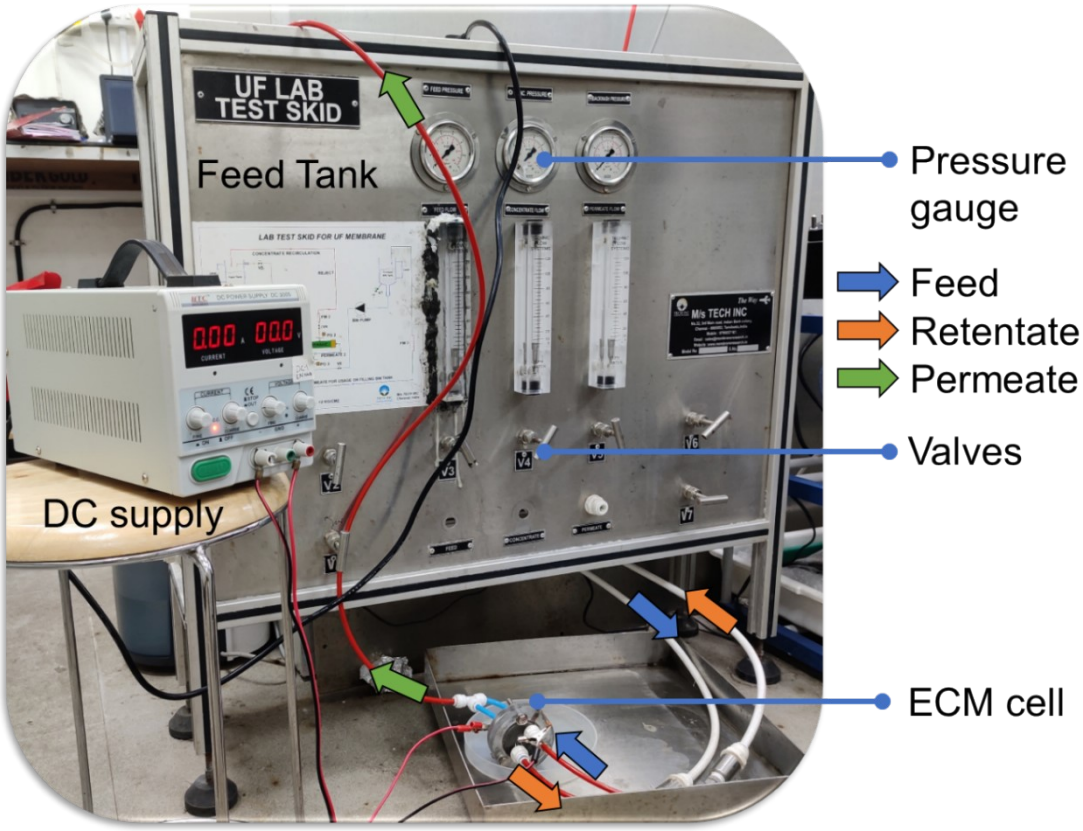

Fig S3: Photograph of the crossflow filtration system

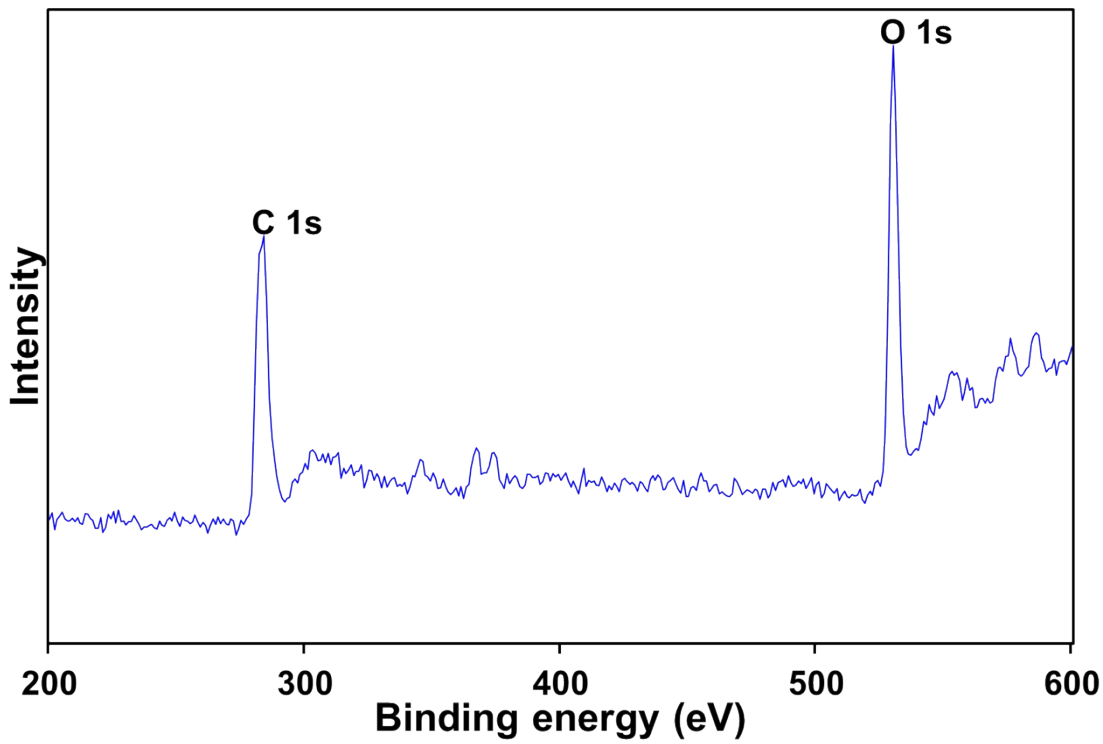

Fig S4: XPS spectrum of LIG filter with no PVA coating

Table S1: Elemental composition of the composite membranes as per XPS data

		BE [eV]	FWHM [eV]	RSF	Atomic conc. [%]	Error [%]	Mass conc. [%]	Error [%]
LIG Filter	C 1s	284.00	5.26	0.28	70.8	1.52	63.5	2.02
	O 1s	530.00	3.99	0.78	27.9	1.39	33.4	1.64
	S 2p	163.00	6.63	0.67	1.3	0.86	3.1	2.02
		BE [eV]	FWHM [eV]	RSF	Atomic conc. [%]	Error [%]	Mass conc. [%]	Error [%]
LIG-PVA 2%	C 1s	283.00	4.05	0.28	75.7	0.73	70.4	0.78
	O 1s	529.00	3.10	0.78	21.8	0.50	27.0	0.59
	N 1s	397.00	3.22	0.48	2.4	0.72	2.6	0.78
		BE [eV]	FWHM [eV]	RSF	Atomic conc. [%]	Error [%]	Mass conc. [%]	Error [%]
LIG-PVA 3%	C 1s	282.00	4.06	0.28	77.2	0.73	72.0	0.78
	O 1s	530.00	3.16	0.78	20.9	0.47	26.0	0.55
	N 1s	397.00	2.86	0.48	1.9	0.73	2.0	0.80
		BE [eV]	FWHM [eV]	RSF	Atomic conc. [%]	Error [%]	Mass conc. [%]	Error [%]
LIG-PVA 4%	C 1s	282.00	4.07	0.28	75.9	0.62	70.6	0.66
	O 1s	529.00	3.02	0.78	20.9	0.44	25.9	0.52
	N 1s	397.00	3.93	0.48	3.3	0.57	3.6	0.62

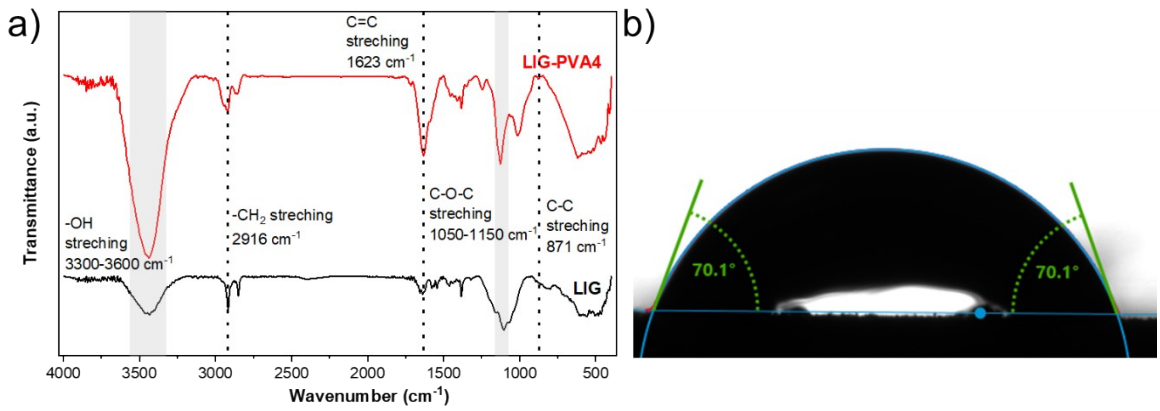

Fig S5: a) FTIR spectrum of LIG and LIG-PVA 4%; Contact angle of LIG filter with no PVA coating.

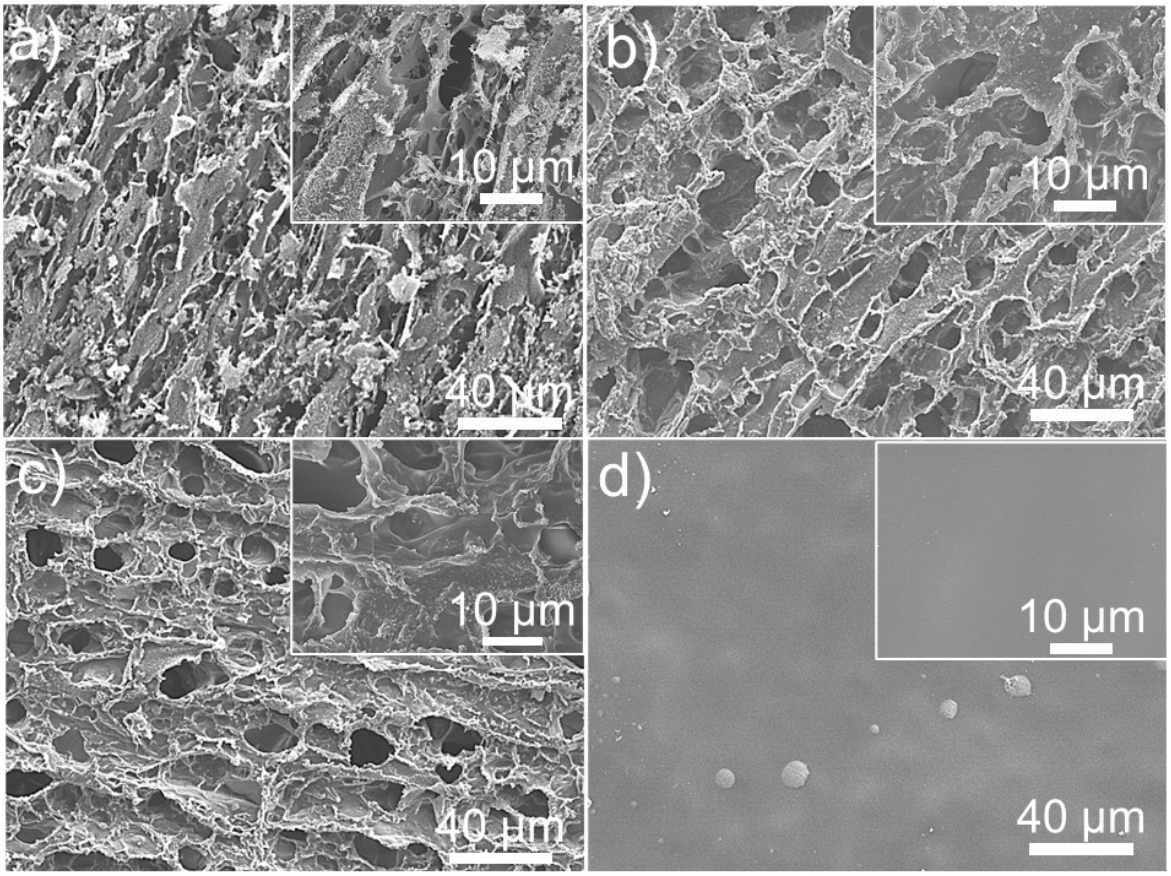

Fig S6: SEM images at 500X magnification (inset 2500X magnification) of: a) LIG; b) LIG-PVA2; c) LIG-PVA3; d) LIG-PVA4

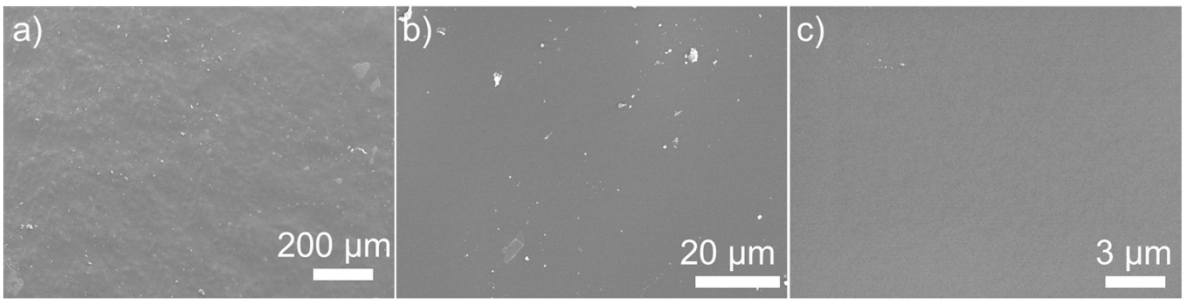

Fig S7: SEM images of LIG-PVA4 at a) 100X; b) 1000X and 5000X magnifications

Text S1

The electrochemical characterization of LIG-PVA composites was also done using cyclic voltammetry (CV), chronoamperometry (CA), and electrochemical impedance spectroscopy (EIS). The CV and CA responses decreased, and the charge transfer resistance increased with an increase in the level of PVA coating (Fig S8). The CV curve area is used to get the surface

charge density (CD)[1,2](Fig S8a). The charge density of LIG-PVA composites was calculated to be 1.33, 1, and 0.66 × 10^4 μC.cm^{-2} for LIG-PVA2, LIG-PVA3, and LIG-PVA4, respectively. The CA plots also showed a similar trend of decrease in CD with the increase in the level of PVA coating (Fig S8b). The EIS data were used to obtain the Nyquist plot to see the effect of PVA coating on the charge transfer resistance of the composites (Fig S8c). From the Nyquist plot, it is observed that with the increase in the level of PVA coating, the semicircular arc is increasing, with LIG-PVA2 showing the lowest semicircular arc, indicating the lower charge transfer resistance. The stability of the LIG-PVA2 composite was also tested for 50 CV cycles and showed only ~10% decrease in the CV response, indicating good stability of the ECMs over the long-run (Fig S8d).

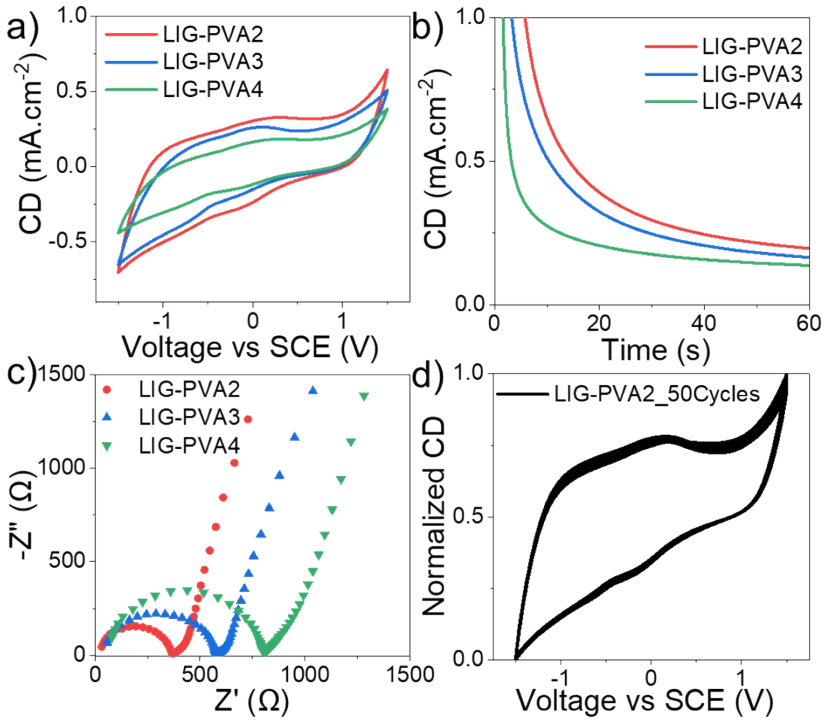

Fig S8: Electrochemical characterization of LIG-PVA composite ECMs. a) Cyclic voltammograms from -1.5 V to 1.5 V at 0.1 V.s^{-1} scan rate; b) chronoamperograms at 1.5 V; c) Nyquist plot for 1000 kHz–0.1 Hz frequency range with 10 mV rms amplitude and d) Cyclic voltammograms of LIG-PVA2 UF ECM for 50 cycles from -1.5 V to 1.5 V at 0.1 V.s^{-1} scan rate. All tests were done with three-electrode system with 0.05 M Na_2SO_4 as the background electrolyte. CD = current density.

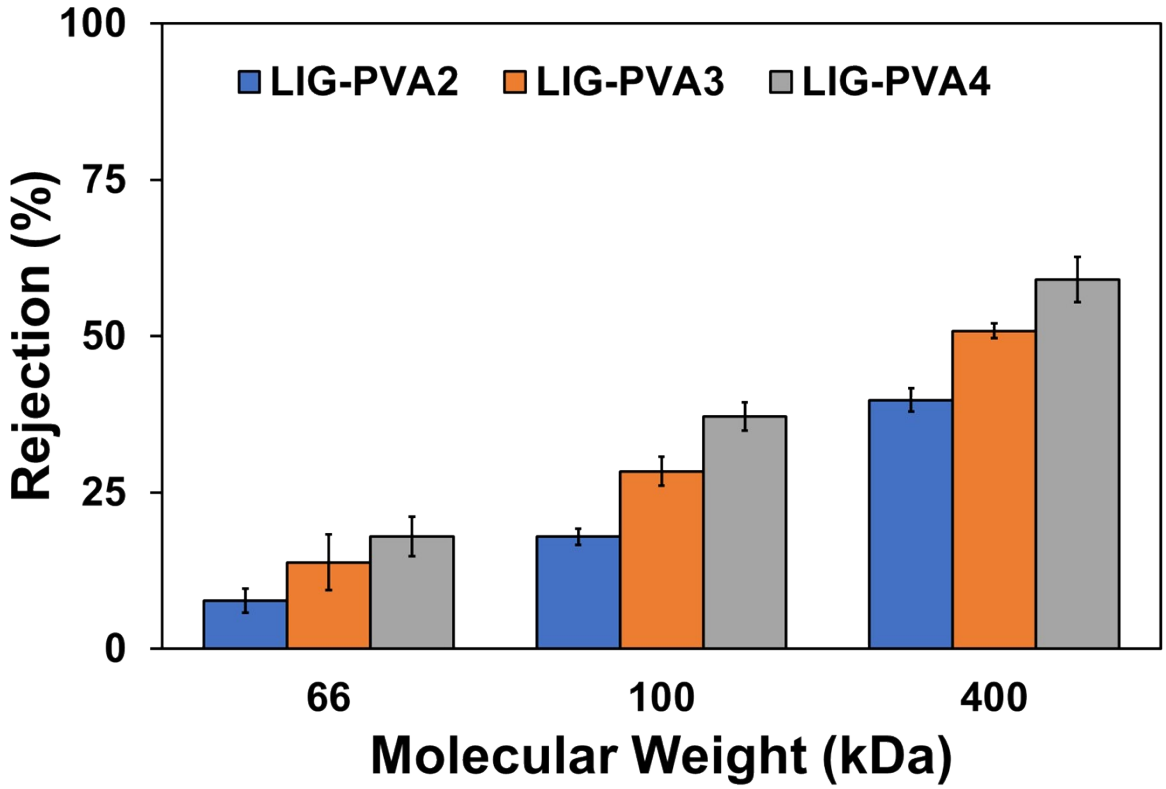

Fig S9: Rejection performance of LIG-PVA composite ECMs with different molecules

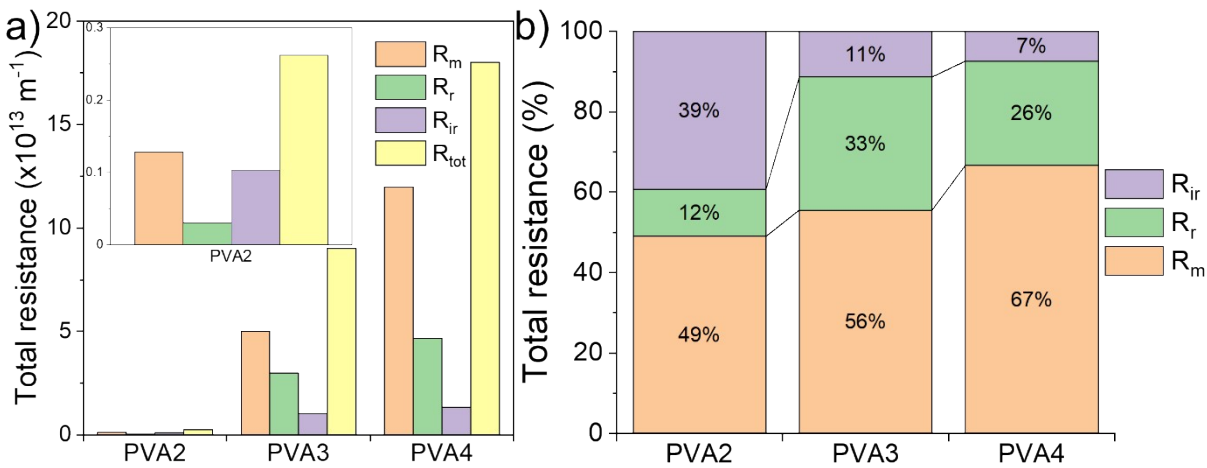

Fig S10: a) Total filtration resistance (R_{tot}) for ECMs including resistance from membrane R_m, reversible R_r, and irreversible fouling resistance (R_{ir}); b) contribution of R_m, R_r, and R_{ir} in total resistance.

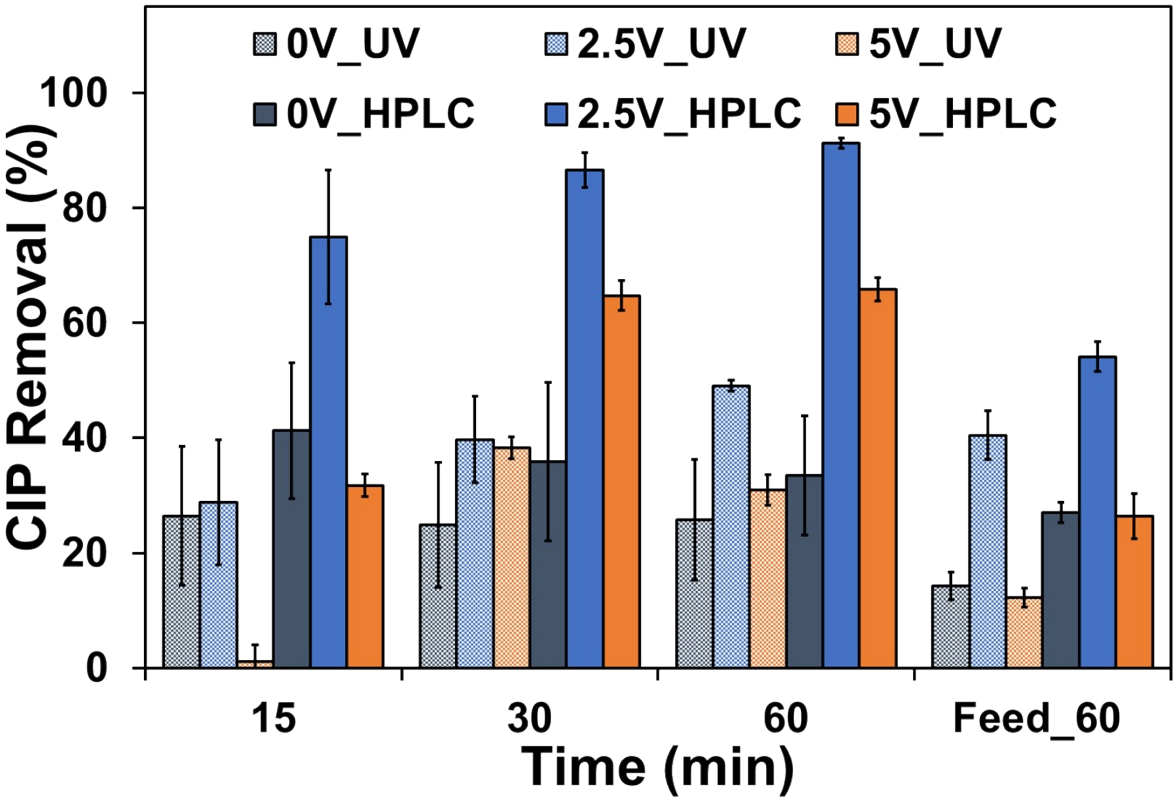

Fig S11: Comparison of UV and HPLC data for CIP removal at different voltages

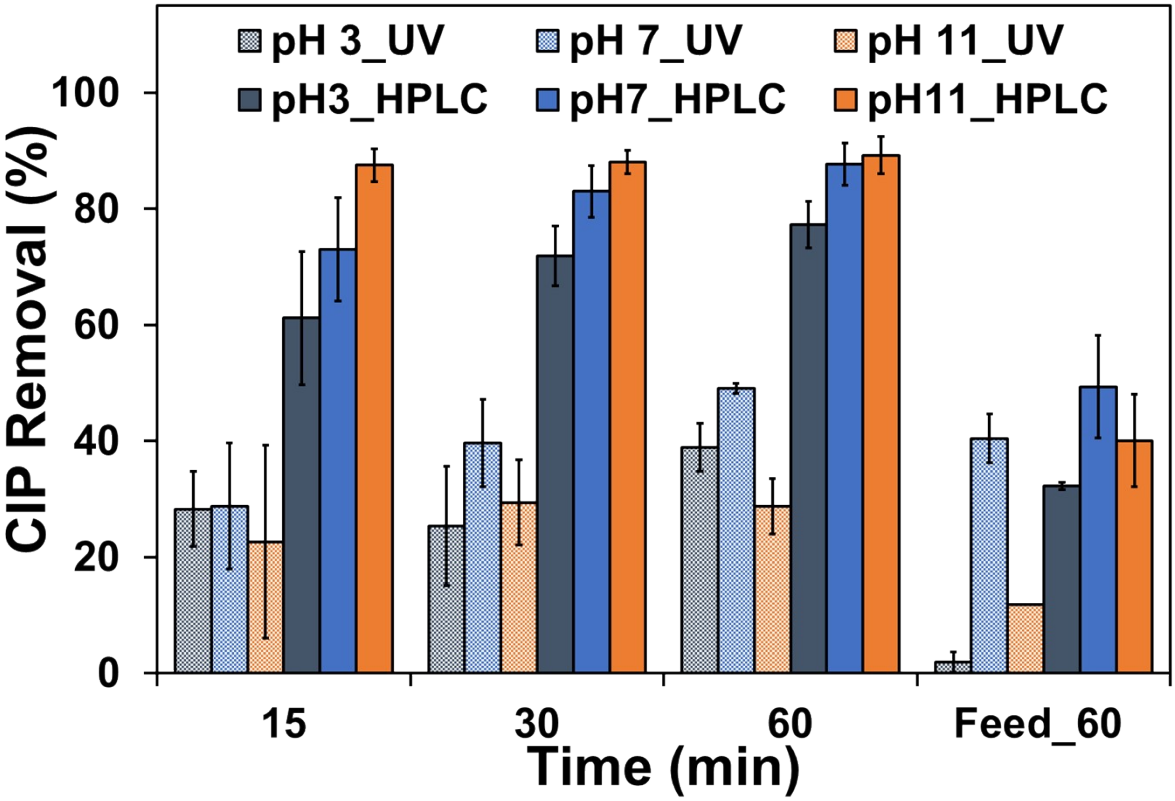

Fig S12: Comparison of UV and HPLC data for CIP removal at 2.5V and different pH values.

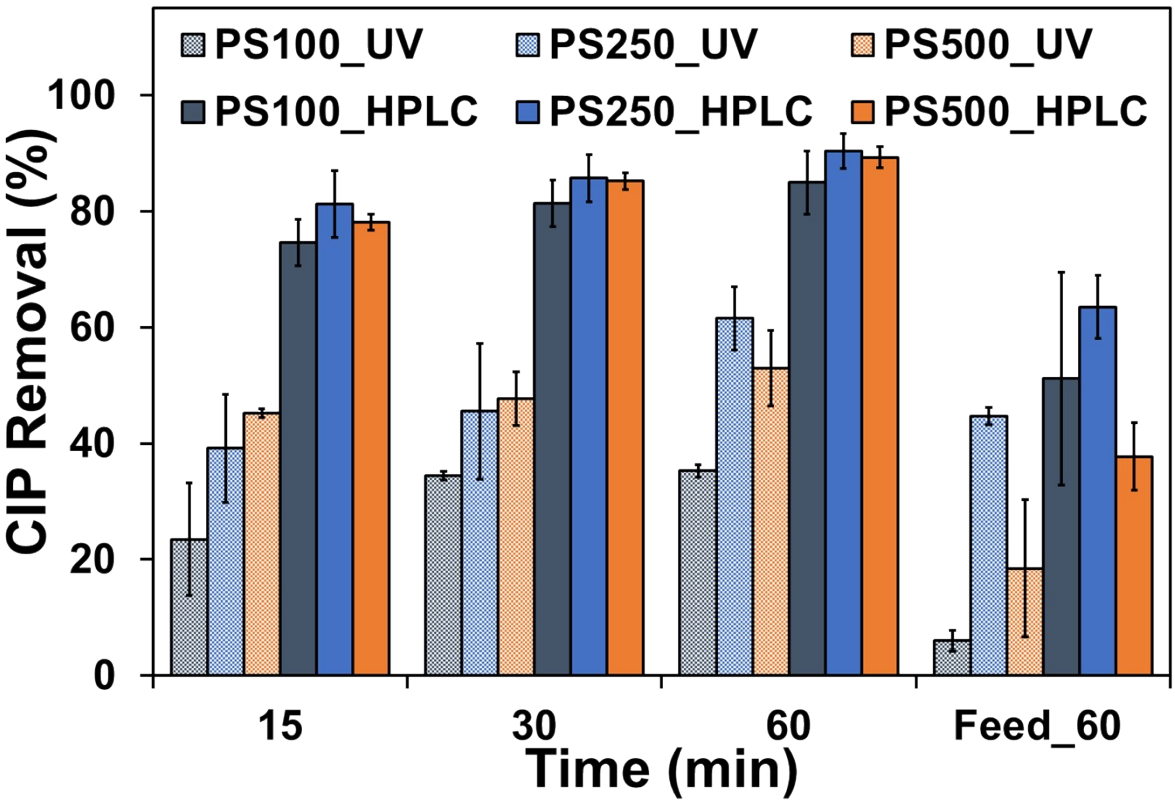

Fig S13: Comparison of UV and HPLC data for CIP removal at 2.5V with different persulfate concentrations

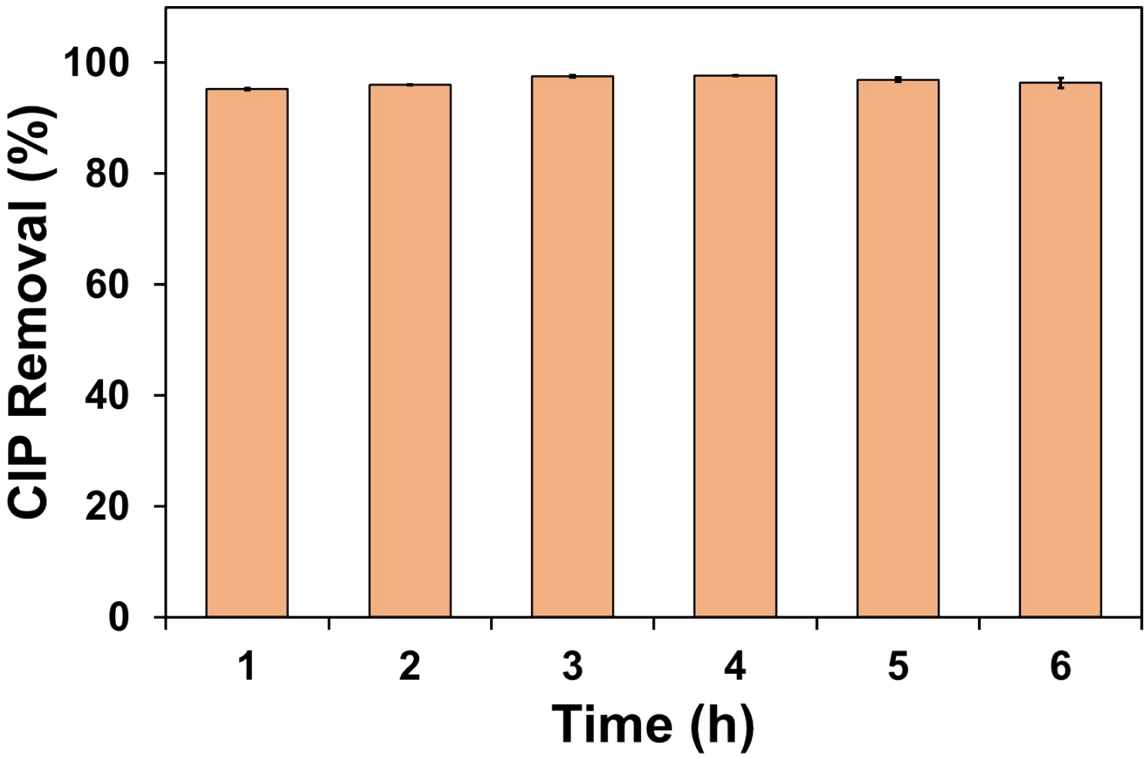

Fig S14: Long-run CIP removal performance of LIG ECM filtration at 2.5 V applied voltage.

Table S2: Recent AOP-based removal studies of Ciprofloxacin

AOP type or catalysts used	Time	Experimental conditions	CIP conc.	CIP removal (%)	Ref.
$Co(NO_3)_2 \cdot 6H_2O$ + PMS	~30 min	reactions carried out in 250 mL beakers with CIP (20 $mg.L^{-1}$, 100 ml) and PMS (0.04 g), initiated by adding 10 mg of catalyst into the CIP solution.	20 $mg.L^{-1}$	96.5	5
HNO_3 + H_2O_2	~24 h	In 250 mL glass beaker 0.4 $g.L^{-1}$ of BC or HNO_3 modified-BC added into 50 mL of 10 $mg.L^{-1}$ CIP solutions at 25 °C, amount of 30% H_2O_2 added (0, 1.0, 3.0 and 5.0 mmol/L), at pH 7).	10 $mg.L^{-1}$	93	6
Thiourea, $Bi(NO_3)_3 \cdot 5\ H_2O$, and $Na_2WO_4 \cdot 2H_2O$ + Xe lamp power: 500 W	~75 min	100 mg photocatalysts and 100 mL CIP (5 $mg.L^{-1}$) solution added to a 250 mL quartz reactor	5 $mg.L^{-1}$	>95	7
Photo-Fenton: H_2O_2 + Fe^{2+}	~90 min	Two 15 W germicidal lamps with maximum emission at 254 nm as radiation source. Iron citrate complex prepared *in situ* resulting in a concentration of 10 μM. H_2O_2 was added to obtain a concentration of 500 μM in the effluent.	0.2 $mg.L^{-1}$	80-95	8
Adsorption-Photo-Fenton.	~ 30 min	Certain amount of catalyst was spiked into 100 mL of CIP solution (20 $mg.L^{-1}$) and stirred vigorously. H_2O_2 was added into above	20 $mg.L^{-1}$	30-89	9

		suspension and simultaneously, the visible light source (300 W Xe lamp equipped with a UV-cutoff filter (λ≥420 nm)) was applied			
$H_2O_2/(Fe^{2+}/Fe^{3+})$/Current	~90-150 min	125 mL of 200 mg.L^{-1} CIP solution containing 0.05 M Na_2SO_4 electrolyzed at current intensity of 18 mA.cm^{-2} at pH 3. 4.0 cm × 5.0 cm RuO_2/Ti mesh electrodes used. In anodic oxidation (AO) process, the anode and cathode were both 4.0 cm × 5.0 cm RuO_2/Ti mesh, while a 4.0 cm × 5.0 cm ACF felt was attached to one of RuO_2/Ti mesh electrodes to act as cathode in EF process.	200 mg.L^{-1}	~90	[10]
$H_2O_2/(Fe^{II}Fe^{III}$ LDH/CF)/Current	90 min	830 mL reactor with $Fe^{II}Fe^{III}$ LDH/CF as a cathode and dimensionally stable anode (DSA, Ti/RuO_2–IrO_2, 11 × 6 cm2) as an anode. Na_2SO_4 was used as electrolyte, 500 mL 0.2 mM CIP solution containing 50 mM Na_2SO_4.	~66 mg.L^{-1}	88	[11]
Medium-Pressure Ultraviolet/Peracetic Acid	~50 min	UV apparatus equipped with a 2.8 kW MPUV lamp at scheduled time intervals, the water sample was withdrawn from the petri dish and was quenched with sodium thiosulfate .	2 mg.L^{-1}	70-95	[12]
Photo Fenton	150 min	3×36 L modules, water flow (58 L. min^{-1}) directly	~0.001	>95%	[13]

		from one module to another and finally to a 100 L tank. Effluent was mixed with 10 mg L^{-1} humic acid. H_2O_2 was added, and after another 15 min, Fe_2SO_4 was added	mg.L^{-1}		
Nanometric MnOOH + PMS	360 min	PMS solution continuously added to the reaction vessel using a peristaltic pump at 0.12 mL min^{-1}. Parameters used pH (3, 7, and 10), MnOOH dosage (0.5, 1.0, and 2.0 g.L^{-1}), and PMS concentration (1, 2, and 4 g.L^{-1}) were evaluated.	50 mg.L^{-1}	>80-95	14
Plasma Fenton system	30 min	DBD plasma was optimally generated at an applied power and airflow of 100 W and 20 L.min^{-1}; operational frequency was ~ 22 kHz.	10 mg.L^{-1}	>92%	15
CuS/ZnO nanosheets/ H_2O_2 system	60 min	aqueous contaminant solution of 50 mL used, addition of 30 mg (0.6 g L^{-1}) of CS/ZO NSs and 50 µL (10 mM) of H_2O_2 to start the reaction. Initial pollutant 10 ppm, initial H_2O_2 10 mM, catalyst 0.6 g. L^{-1}, and initial anions 20 mM.	10 mg.L^{-1}	>99%	16
Hydrodynamic cavitation with P-doped TiO_2 catalysts	120 min	Batch experiments using 5 L of CIP, photocatalytic experiments done with catalyst dose of 0.5 g L^{-1}, pH value 3-11. Three different CIP concentrations (5, 10, 15 mg L^{-1}), and P/Ti	5-15 mg.L^{-1}	~91%	17

		molar ratios of 0.02, 0.04, 0.06.			
UV/chlorine	10 min	CIP (50 μM) removal by UV/chlorine was triggered with 100 mL samples, certain volume of NaClO stock solution	~16.5 $mg.L^{-1}$	>73%	[18]
novel FeS_2/biochar catalyst-based Fenton system	20 min	FeS_2/BC and H_2O_2 were put into CIP solution. Concentrations of CIP, FeS_2/BC and H_2O_2 were 30 mg L^{-1}, 1.5 g L^{-1}, and 5 mM, respectively.	30 $mg.L^{-1}$	~97%	[19]
Zn-MOF + PMS	60 min	0.1 mM PMS was added into the reaction solution that contain 10 $mg.L^{-1}$ of CIP. Reaction started after 0.4 $g{\cdot}L^{-1}$ of ZIF-65/PAN added	10 $mg.L^{-1}$	~89%	[20]
Present Study (ECM and Fenton incorporated ECM)	15-60 min	Applied voltage 2.5V, permeate flow rate ~100 LMH	10 $mg.L^{-1}$, 0.5 $mg.L^{-1}$	≥70-90%	This study

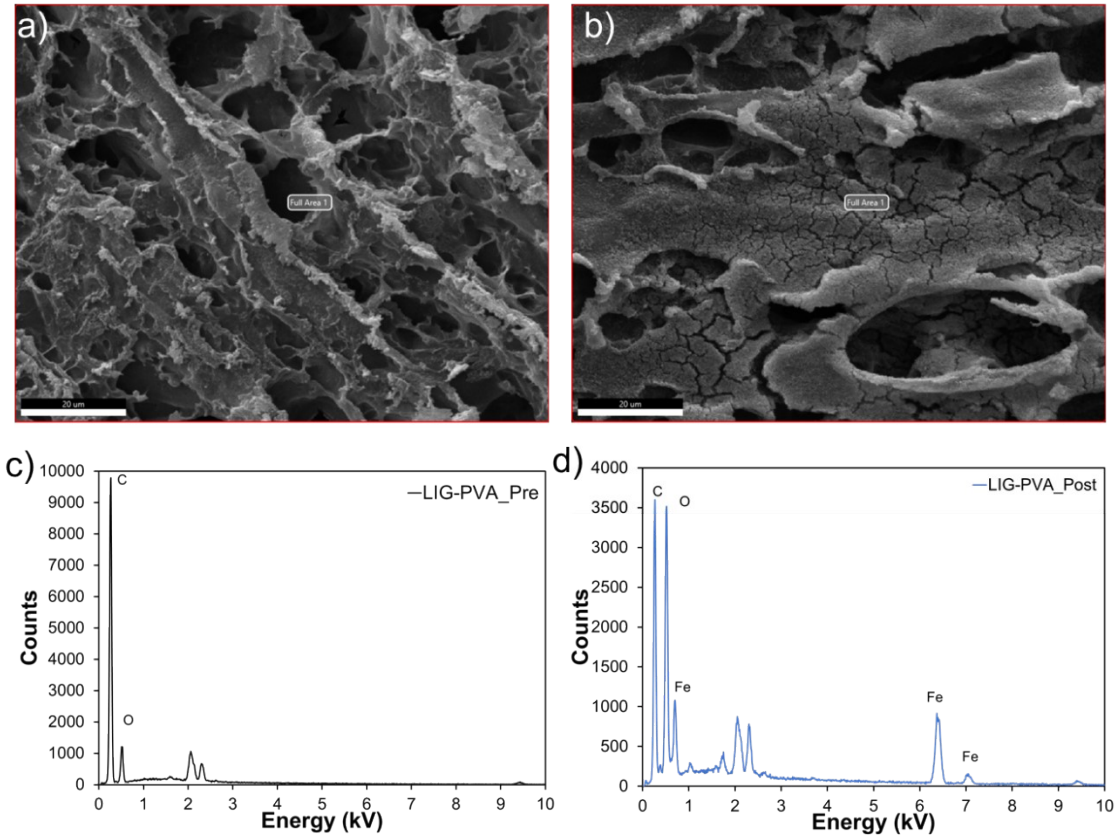

Fig S15: SEM-EDS spectrum of LIG-PVA composite pre and post-filtration.

Table S3: EDS elemental composition of LIG-PVA composite pre and post filtration

LIG-PVA	**Element**	**Weight %**	**Atomic %**
Pre-reaction	C	87.0	90.0
	O	12.9	10.0
	Fe	0.2	0.0
Post-reaction	C	56.3	69.8
	O	28.0	26.1
	Fe	15.7	4.2

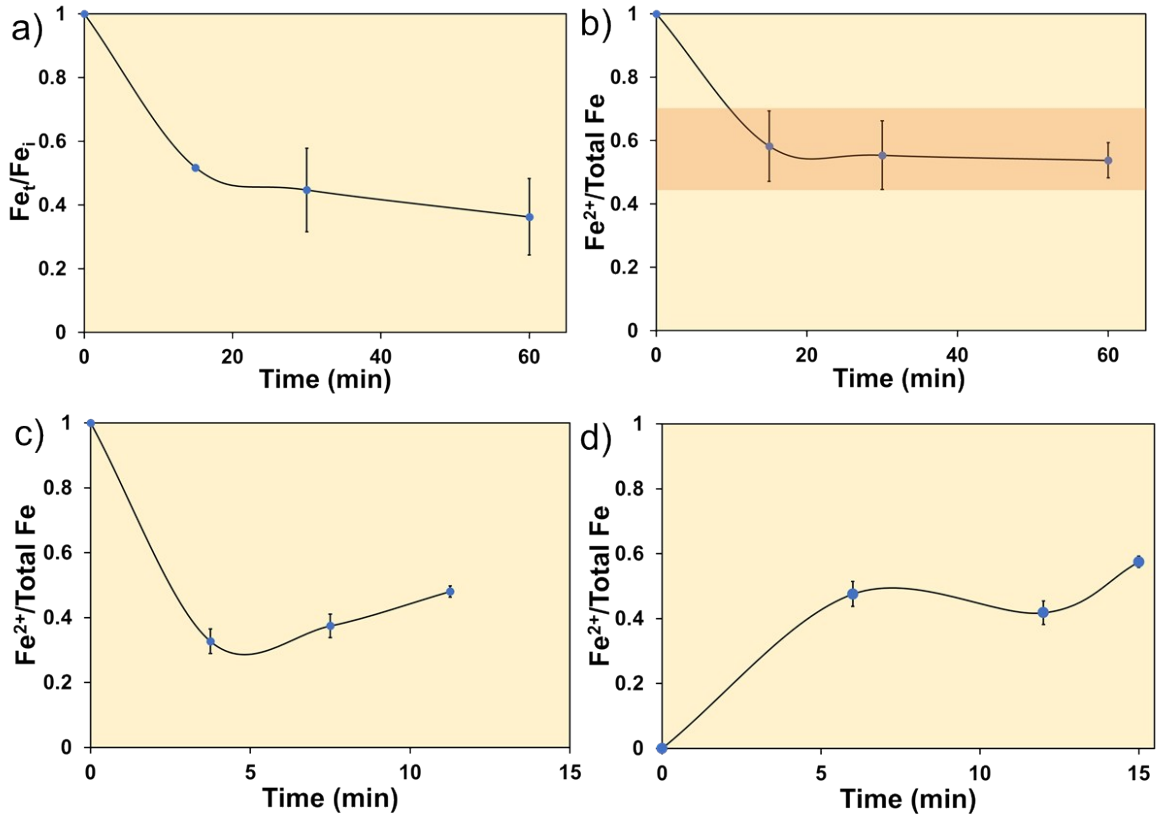

Fig S16: a) Total Fe concentration and b) Fe^{2+}/Total Fe with time in crossflow filtration with 10 mg.L^{-1} CIP, PS100, Fe10, and 2.5V. c) Fe^{2+}/Total Fe in dead-end filtration mode with 10 mg.L^{-1} CIP, PS100, Fe10, and 2.5V d) Fe^{2+}/Total Fe in dead-end filtration mode with ferric chloride only at 2.5V.

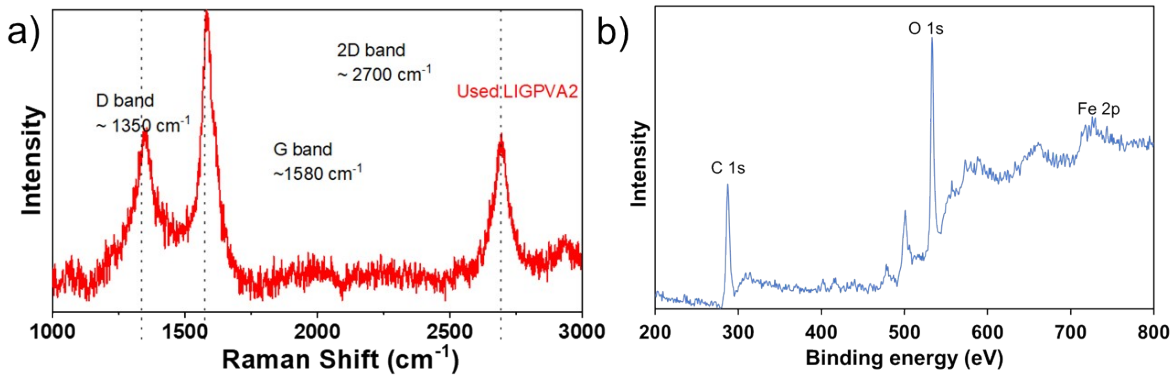

Fig S17: a) Raman and b) XPS spectra of LIG-PVA after filtration.

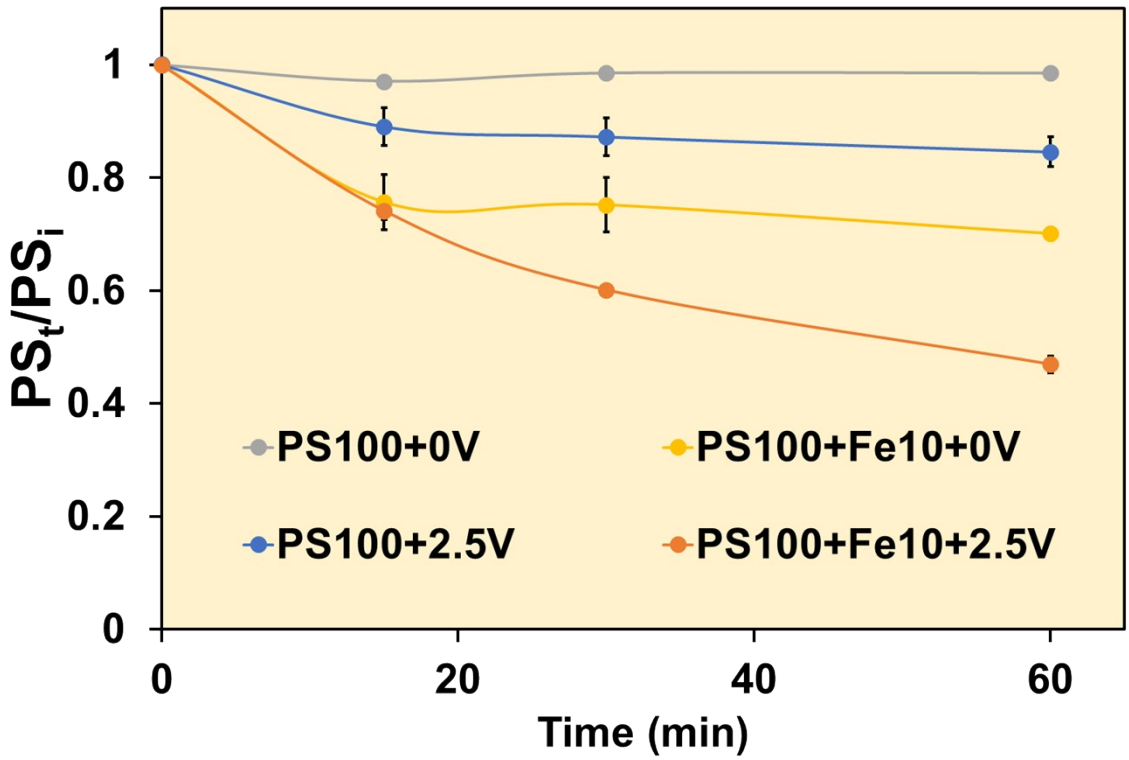

Fig S18: Persulfate concentration with filtration time

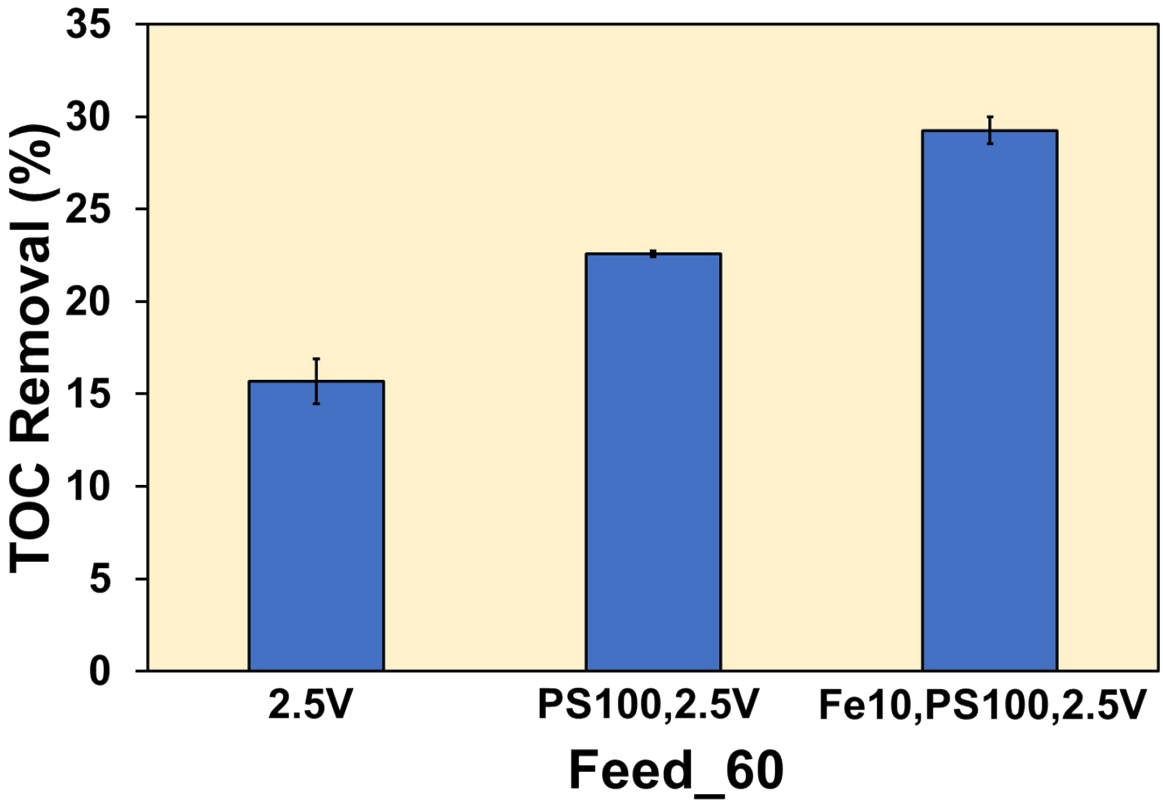

Fig S19: TOC removal by the ECM filtration system. CIP = 10 mg.L^{-1}; PS100, Fe10, 2.5V.

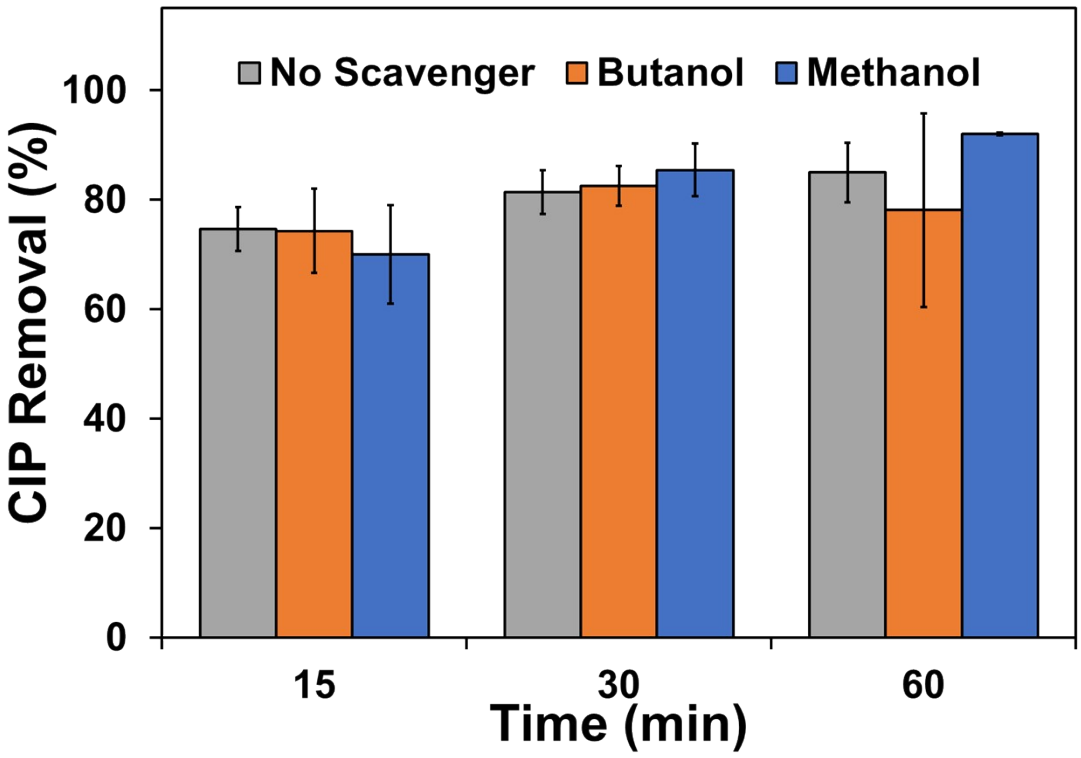

Fig S20: CIP removal in presence of scavengers at pH7, 2.5V and PS100

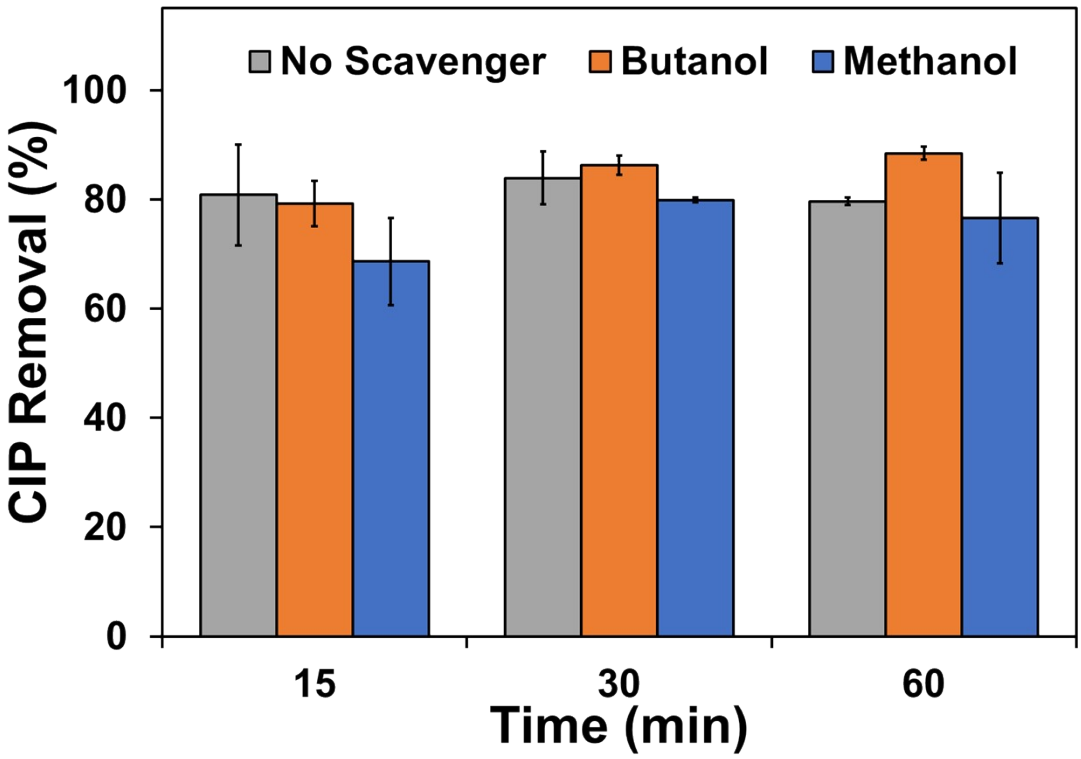

Fig S21: CIP removal in presence of scavengers at pH7, 2.5V, PS100 and Fe10

Table S4: Composition of synthetic municipal wastewater used in the study[21–24]

Component	Concentration ($mg.L^{-1}$)
Glucose	400 ± 10
$NaHCO_3$	24 ± 5
K_2HPO_4	18 ± 5
NH_4Cl	60 ± 5
$MgSO_4.7H_2O$	72 ± 3
$CaCl_2.2H_2O$	40 ± 3

Table S5: m/z values and the structure of degradation products of CIP

Sl. No.	m/z	Structure
1	332	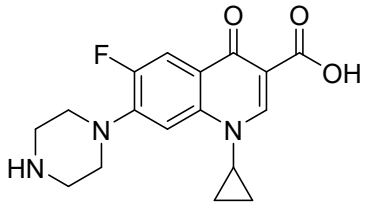
2	306	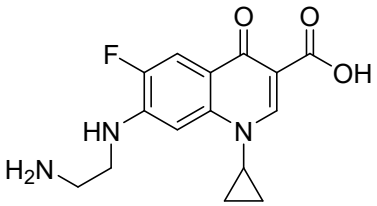
3	274	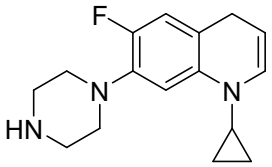
4	263	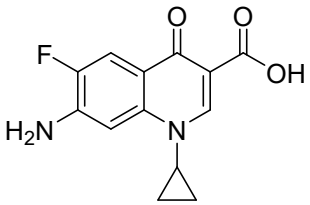

5	160	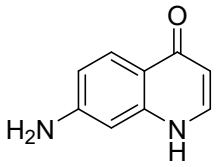

References

1 A. Kumar, N. H. Barbhuiya and S. P. Singh, *Chemosphere*, 2022, 307, 135878.

2 A. Kumar, N. H. Barbhuiya, A. M. Nair, K. Jashrapuria, N. Dixit and S. P. Singh, *Chemosphere*, 2023, **335**, 138988.

3 W. Zhai, H. Yu, H. Chen, L. Li, D. Li, Y. Zhang and T. He, *Sep. Purif. Technol.*, 2022, **293**, 121091.

4 N. Sreedhar, N. Thomas, O. Al-Ketan, R. Rowshan, R. K. Abu Al-Rub, S. Hong and H. A. Arafat, *J. Memb. Sci.*, 2020, **616**, 118571.

5 J. Luo, S. Bo, Y. Qin, Q. An, Z. Xiao and S. Zhai, *Chem. Eng. J.*, 2020, **395**, 125063.

6 K. Luo, Q. Yang, Y. Pang, D. Wang, X. Li, M. Lei and Q. Huang, *Chem. Eng. J.*, 2019, **374**, 520–530.

7 W. Mao, L. Zhang, Y. Liu, T. Wang, Y. Bai and Y. Guan, *Chemosphere*, 2021, **263**, 127988.

8 J. A. L. Perini, A. L. Tonetti, C. Vidal, C. C. Montagner and R. F. P. Nogueira, *Appl. Catal. B Environ.*, 2018, **224**, 761–771.

9 Q. Wu, M. S. Siddique, Y. Guo, M. Wu, Y. Yang and H. Yang, *Appl. Catal. B Environ.*, 2021, **286**, 119950.

10 Y. Chen, A. Wang, Y. Zhang, R. Bao, X. Tian and J. Li, *Electrochim. Acta*, 2017, **256**, 185–195.

11 B. Yao, Z. Luo, J. Yang, D. Zhi and Y. Zhou, *Environ. Res.*, 2021, **197**, 111144.

12 X. Ao, X. Zhang, S. Li, Y. Yang, W. Sun and Z. Li, *J. Hazard. Mater.*, 2023, **445**, 130480.

13 N. Klamerth, S. Malato, A. Agüera and A. Fernández-Alba, *Water Res.*, 2013, **47**, 833–840.

14 Y. Núñez-de la Rosa, L. G. C. Durango, M. R. Forim, O. R. Nascimento, P. Hammer and J. M. Aquino, *Appl. Catal. B Environ.*, 2023, **327**, 122439.

15 S. H. Kim, J. Seo, Y. Hong, Y. Shin, H.-J. Chung, H.-R. An, C. Kim, J.-I. Park and H. U. Lee, *J. Water Process Eng.*, 2023, **52**, 103519.

16 T. Gao, H. Wang, J. Xu, C. Hu and L. Lyu, *ACS ES T Water*, 2023, **3**, 79–85.

17 M. Chen, K. Zhuang, J. Sui, C. Sun, Y. Song and N. Jin, *Ultrason. Sonochem.*, 2023, **92**, 106265.

18 Y. Shao, X. Li, L. Jiang, X. Wei, Y. Zhao, X. Chen and S. Li, *J. Clean. Prod.*, 2022, **379**, 134482.

19 F. Sang, Z. Yin, W. Wang, E. Almatrafi, Y. Wang, B. Zhao, J. Gong, C. Zhou, C. Zhang, G. Zeng and B. Song, *J. Clean. Prod.*, 2022, **378**, 134459.

20 M. Pu, D. Ye, J. Wan, B. Xu, W. Sun and W. Li, *Sep. Purif. Technol.*, 2022, **299**, 121716.

21 S. Ahmadzadeh and M. Dolatabadi, *J. Mol. Liq.*, 2018, 254, 76–82.

22 B. M. B. Ensano, L. Borea, V. Naddeo, V. Belgiorno, M. D. G. de Luna and F. C. Ballesteros, *Water (Switzerland)*, 2017, **9**, 1–15.

23 M. Prado, L. Borea, A. Cesaro, H. Liu, V. Naddeo, V. Belgiorno and F. Ballesteros, *Int. Biodeterior. Biodegrad.*, 2017, **119**, 577–586.

24 A. Reza and L. Chen, , DOI:10.3390/pr9112059.